Properties of PET Fibers with High Modulus and Low Shrinkage (HMLS). I. Yarn Properties and Morphology

P. B. RIM* and C. J. NELSON

Allied-Signal Corporation, Fibers Division Technical Center, Petersburg, Virginia 23804

SYNOPSIS

Classical morphological analysis has been performed on novel PET fibers of high modulus and low shrinkage (HMLS). As expected, amorphous orientation controls the degree of shrinkage and tenacity. The uniqueness of these materials is derived from a high "effective" crosslink density which results in a high retractive force during elevated temperature shrinkage and significant stress-amplification during room temperature extension. Although the morphological origin of the high effective crosslink density is unknown, it is speculated that the interfibrillar regions contribute to the observed behavior by suppressing yielding.

INTRODUCTION

PET fibers of high modulus and tenacity are used in industrial applications such as reinforcements for rubber articles (i.e., tires and hoses), geotextiles, ropes, and cordage. The importance of this thermoplastic fiber in the marketplace has consequently generated much fundamental research concerned with the relationship between processing, morphology, and physical properties. Early work is discussed in a text by Samuels.[1] He emphasizes the two-phase nature of PET fibers and describes "universal" relationships between amorphous orientation and mechanical properties after accounting for crystallinity differences between samples. Although the presence of a third, interfibrillar phase has sometimes been adopted to explain particular phenomena, the two-phase approach remains the foundation of recent work.[2-9]

In this paper we will provide an analysis of structure/property relations for novel PET yarns possessing the special characteristics of high modulus and low shrinkage (HMLS). Yarns with this somewhat unique combination of properties have been prepared previously by subjecting drawn yarns to thermal treatment procedures, and research has been devoted to understanding associated morphological changes.[2,3,5,10] The fibers of this investigation are unique in that no thermal treatment is necessary to achieve the low shrinkage. The current yarns are also unique in that they exhibit a high degree of stress-amplification during extension. This is extremely desirable for applications like tire cords in which the fibers are continuously strained 2–5%.

The properties of tire cords prepared from these yarns will be presented in Part II of this series. It will be shown that the fundamental yarn characteristics described here are translated to the tire cord form, even after the extensive heat treatment associated with cord formation.

EXPERIMENTAL

Yarns

Yarns studied are produced by Allied-Signal and are designated 1W70, 1W90, and A330. Intrinsic viscosities, as measured in a 60/40 (wt %) mixture of phenol and tetrachloroethane, fall within the 0.88–0.91 range. 1W70 is a conventional high modulus and high tenacity fiber, and 1W90 is a dimensionally stable yarn used in applications which demand high modulus and low shrinkage. A330 is a recently introduced yarn of advanced dimensional stability. These yarns were drawn near the maximum draw ratio under similar heat histories, and were not subjected to a thermal treatment. A minimal relaxation step occurred after drawing. Yarn denier and filament count were 1000d and 300f, respectively with

* To whom correspondence should be addressed.

Journal of Applied Polymer Science, Vol. 42, 1807–1813 (1991)

 CCC 0021-8995/91/071807-07$04.00

the exception of 1W70 which possessed 192 filaments.

Static Mechanical Properties/Shrinkage

Tensile measurements were performed using a Model 1125 Instron at a strain rate of 120%. Initial modulus, ultimate elongation (UE), and tenacity were taken as usual. The stress-amplification upon elongation was measured as the "load at a specified elongation of 5%" (LASE-5). All data cited is the average of 10 runs.

Shrinkage was determined under loads of 5–100g at 177°C. Measurements were taken at "equilibrium" which occurred after approximately 1 min. Retractive force values were taken as the maximum of the retractive force vs. time curve at 177°C.

Dynamic Mechanical Properties

Dynamic mechanical properties were measured on a Rheometrics RSAII analyzer at a frequency of 10 Hz and a thermal scan rate of 1.6°C/min. The yarns were pretensioned at 250g and the strain amplitude was maintained at 0.17%

Morphological Characterization

Density was measured in a n-heptane/carbon tetrachloride density gradient column at 23°C.

Thermal analysis was performed with a Perkin-Elmer DSC-7 equipped with a data station. Melting points (T_m) were taken at the peak of the melting endotherm. Small samples (2 mg) were used for T_m analysis for enhanced resolution and accurate temperature measurement. Large samples were tested for heat of fusion determination.

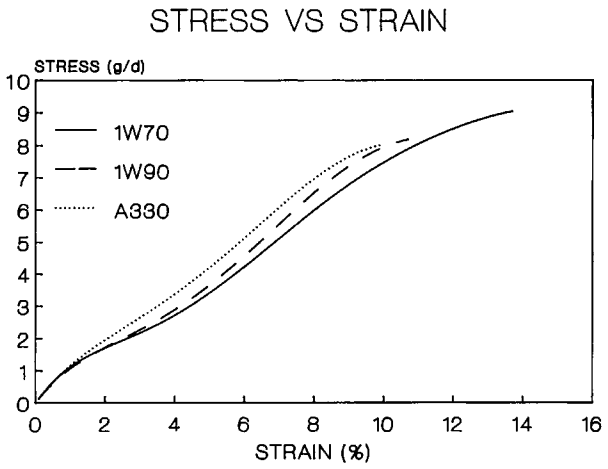

Figure 1 Representative stress vs. strain curves for 1W70, 1W90, and A330.

Table I Tensile Properties of PET Fibers

Property	1W70	1W90	A330
Tenacity (g/d)	9.2	8.1	7.9
Initial modulus (g/d)	112	98	100
LASE-5 (g/d)	3.62	3.67	4.14
SAR	0.65	0.75	0.83
Ultimate elongation (%)	13.7	11.1	10.5
Shrinkage*(%)	12.5	9.6	7.5
Retractive force (g/d)	0.32	0.32	0.35

* Tension 9g.

Wide-angle x-ray scattering (WAXS) was measured using a Philips vertical goniometer with CuKα radiation generated at 45 kV and 35 mA. Resolution of overlapping peaks was accomplished with a profile curve fitting program provided by Philips. Small-angle x-ray scattering (SAXS) was kindly measured by N. S. Murthy employing a Franks' camera and a 1-D position sensitive detector.

Birefringence measurements were made with a Leitz Model NR 5533 polarizing microscope employing a 23-order berek compensator.

Sonic modulus measurements were made on a Morgan Dynamic Modulus Tester Model PPM5 at a frequency of 5 kc/sec.

RESULTS AND DISCUSSION

Tensile Properties/Shrinkage

Representative stress–strain curves for the 3 yarns of this investigation, 1W70, 1W90, and A330, are depicted in Figure 1 and data derived from these traces is summarized in Table I along with representative shrinkage and retractive force results. The conventional 1W70 yarn possesses the highest modulus but the lowest load at 5% elongation (LASE-5). To quantify this behavior a stress-amplification ratio (SAR) was defined as the secant modulus at 5% elongation (i.e., LASE-5/0.05) divided by the initial modulus. As indicated in Table I, SAR follows the order A330 > 1W90 > 1W70. Evaluating the stress–strain response as instantaneous modulus–strain curves serves to further emphasize this observation (Fig. 2). A330 shows the desired feature of a more nearly constant modulus at low strains. In fact, A330 has a 50% higher modulus than 1W70

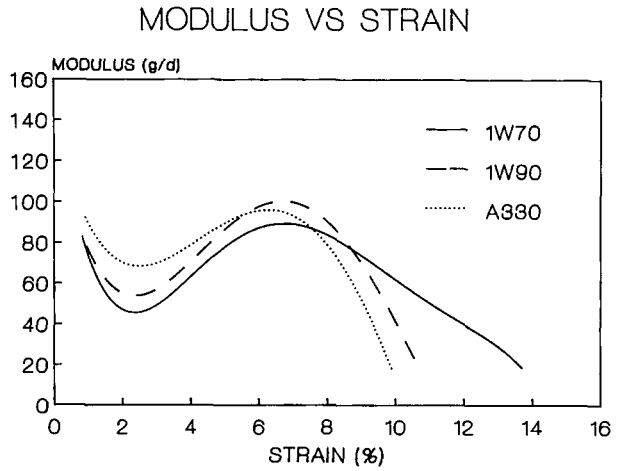

Figure 2 Representative modulus vs. strain curves depicting stress amplification for 1W90 and A330.

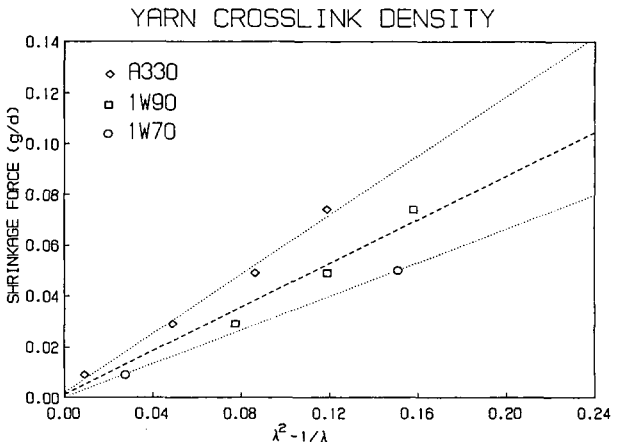

Figure 4 Plot of shrinkage force vs. $\lambda^2 - 1/\lambda$ derived from rubber elasticity theory.

at 2.2% strain. If one attributes the reduction in modulus at 1–3% strain to yielding, then it seems reasonable to attribute the more linear behavior to a suppression of this yielding.

Tenacity exhibits the opposite trend as SAR, with 1W70 and A330 possessing the largest and smallest values, respectively. Shrinkage at 177°C as a function of constraining force is plotted in Figure 3 and the trend is the same as that for tenacity. Therefore, A330 exhibits the paradoxical, yet desirable characteristics of high LASE-5 and low shrinkage.

Although one would expect retractive force to mimic the shrinkage values, this parameter is relatively invariant between the samples (Table I). It is instructive to further analyze the shrinkage vs. constraining force plot of Figure 3 and derive the inherent retractive force of the samples independent

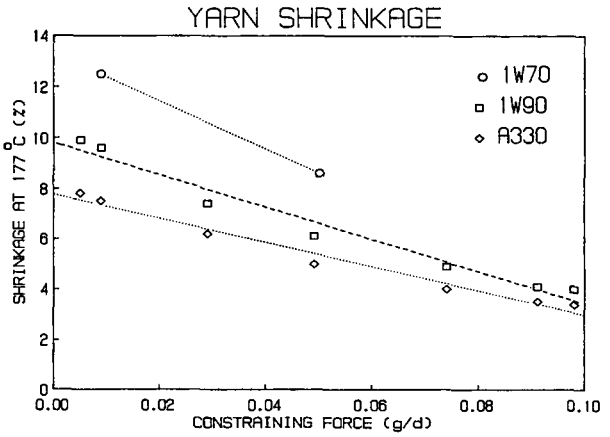

Figure 3 Plot of shrinkage measured at 177°C vs. constraining force.

of shrinkage differences. For example, if one assumes that the crystals or tie chains of a semicrystalline polymer are analogous to the crosslinks of a rubber, the kinetic theory of rubber elasticity can be applied to shrinkage/constraining force data to compute an effective crosslink density. The relationship of interest is[11–13]

$$\sigma = NkT(\lambda^2 - 1/\lambda) \qquad (1)$$

where σ = shrinkage or constraining force, k = Boltzmann constant, T = temperature, λ = extension ratio, and N = network chains/cc. Application of this equation to shrinkage data at various constraining forces assumes that the material shrinks to the extent that the shrinkage force equals the constraining force. The extension ratio (λ) then becomes $1/(1 - (S_0 - S_c))$, where S_0 is the shrinkage at minimal constraining force and S_c is the shrinkage at the constraining (shrinkage) force of interest. Plots derived from eq. (1) are depicted in Figure 4. Values for N, the effective number of crosslinks or network chains/cc are calculated from the slope giving 6.6, 8.5, and 11.5×10^{21} for 1W70, 1W90, and A330, respectively. Increases in N can be envisioned to arise because of increased number of crystals, increased direct crystal–crystal connectivity, or increased crystal–crystal connectivity thru tie chains. These possibilities will be discussed further in the next section.

Regardless of the mechanism, the behavior of N is consistent with the stress-amplification observed in the stress–strain measurements, suggesting these two parameters are controlled by the same morphological characteristic(s).

Morphological Analysis

The results of thermal analysis, dilatometry, birefringence, sonic measurements, and x-ray scattering are provided in Table II. Crystallinity values were calculated from both the DSC traces (Fig. 5) and the density data. The calorimetrically derived values (X_c) were calculated assuming a perfect heat of fusion of 140 J/g[14] and the density derived values (X_d) were computed as follows[15]

$$X_d = \frac{\rho_c(\rho - \rho_a)}{\rho(\rho_c - \rho_a)} \quad (2)$$

where ρ = overall density, ρ_a = intrinsic amorphous density, and ρ_c = intrinsic crystal density. Values of ρ_a and ρ_c were taken as 1.335 and 1.495 g/cc, respectively.[16,17]

Good agreement exists between the crystallinity values calculated from the two approaches. However, this may be fortuitous since X_d is highly dependent on the value chosen for ρ_c. Nevertheless, it is clear that the relative extent of crystallinity does not vary much from sample to sample, as expected of highly drawn fibers. Melting point tends to increase as the yarn dimensional stability increases. DSC analysis at varying heating rates confirmed that these differences are sample characteristics rather than a function of the test procedure.

Amorphous orientation (f_a) was calculated from the birefringence results as follows[18]

$$f_a = \frac{\Delta_t - (X)(\Delta_c^o)(f_c)}{(1 - X)\Delta_a^o} \quad (3)$$

where Δ_t = overall birefringence, X = percent crystallinity, f_c = crystal orientation, Δ_c^o = intrinsic crystal birefringence (0.220), and Δ_a^o = intrinsic amorphous birefringence (0.275). f_c was determined from an azimuthal scan of the 105 reflection.[19]

Table II Morphological Analysis

Parameter	1W70	1W90	A330
T_m (°C)	256.1	257.5	259.1
X_c (%)	35	37	38
X_L (%)	61	65	75
ρ (g/cc)	1.3898	1.3857	1.3864
X_d (%)	37	34	35
Δn	0.2322	0.2026	0.1972
f_a	0.88	0.71	0.68
L (Å)	136	113	106
L_a (Å)	53	39	26
L010 (Å)	57	54	57
L1$\bar{1}$0 (Å)	52	45	47
L100 (Å)	43	42	42
L$\bar{1}$05 (Å)	83	74	80

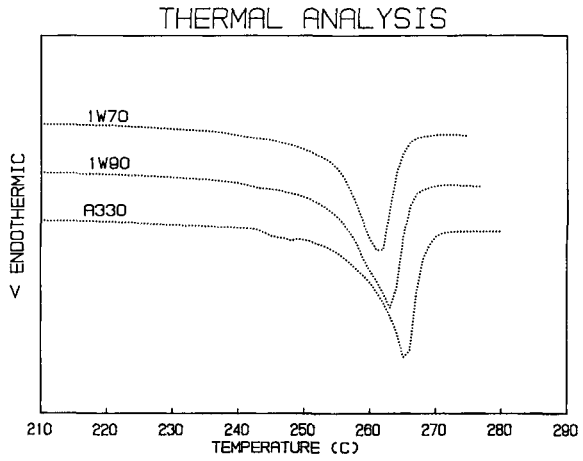

Figure 5 Typical DSC traces for 10-mg samples tested at 20°C/min.

Figure 6 depicts the expected relation between shrinkage and f_a. Tenacity, sonic modulus, and LASE-5 are plotted vs. f_a for the 3 yarns of interest in Figures 7, 8, and 9. Also included in these figures is data for a series of 1W90 yarns prepared at different draw ratios. These additional results are added to enhance the accuracy of the trends. Both tenacity and sonic modulus increase with f_a as expected, and the different type yarns fall on the same line. The similar dependence of sonic modulus on f_a for all the samples is attributed to the "conventional" dependence of modulus on amorphous orientation at very low strains. This contrasts the LASE data of Figure 9, which indicates that both

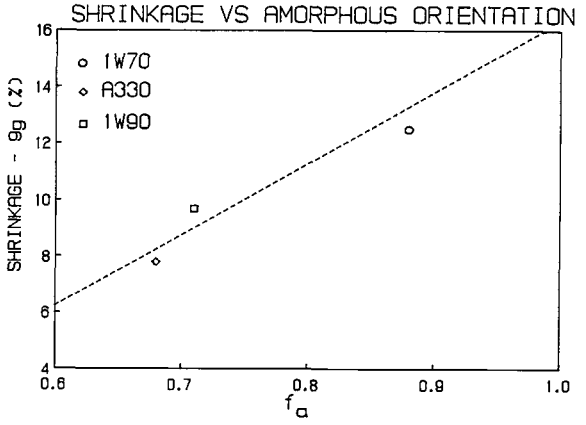

Figure 6 Plot depicting the relationship between f_a and shrinkage under $9g$ load.

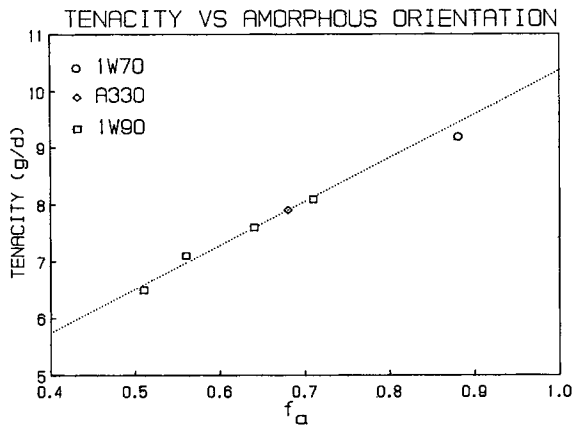

Figure 7 Plot depicting the relationship between f_a and tenacity.

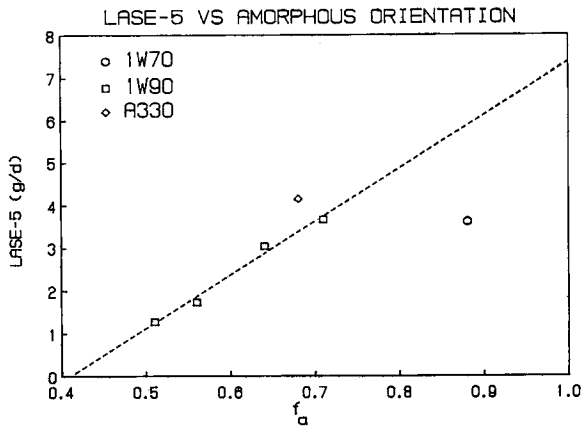

Figure 9 Plot of LASE-5 vs. f_a showing the superior LASE-5 at a given f_a for 1W90 and A330.

A330 and 1X90 exhibit an elevated LASE-5 at a given f_a when compared to "conventional" 1W70. This observation is analogous to the previously mentioned stress-amplification. The initial modulus values, which represent "averaging" from 0–1% strain, are less strongly dependent on f_a than the sonic values. Hence, initial modulus seems to be influenced by the stress-amplification mechanism. This is further reinforced by our unpublished hysteresis measurements on similar conventional and HMLS yarns. The latter exhibited lower hysteresis and less permanent set when cycled from 0–0.5% strain. This more elastic behavior for HMLS yarns is consistent with the suppression of yielding previously discussed.

Extrapolation of the tenacity line in Figure 7 gives a value of 10.4 g/d for perfect orientation ($f_a = 1.0$). This should be the maximum tenacity achievable with this molecular weight polymer. However, ultradrawing studies on this polymer yielded a tenacity of 11 g/d suggesting an upturn in the curve above ($f_a = 0.9$).

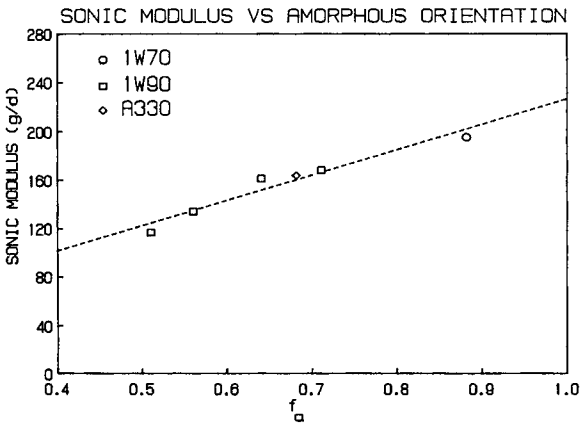

Figure 8 Plot depicting the relationship between f_a and sonic modulus.

Lateral crystallite sizes (L) were determined for the equatorial peaks at 17°, 23°, and 26° 2θ (010, $1\bar{1}0$, 100 reflections[20]) and longitudinal crystallite size was estimated from the nearly meridional peak at 43° 2θ ($\bar{1}05$ reflection).[19] Assuming Gaussian line shapes, the Scherrer equation[21] was used to compute crystal sizes as follows

$$L = \frac{k\lambda}{\beta \cos(2\theta/2)} \tag{4}$$

where L = crystal size, k = shape factor (~ 1.0), λ = wave length of x-rays, β = width at half-height of reflection, and 2θ = Bragg angle. Good collimation eliminated the need for instrument broadening corrections.

Long periods (L) were calculated from the peak of the SAXS reflection.[22] Although no distinguishing features are evident from the crystallite size data alone, combined analysis of the long period and longitudinal crystal size data is informative. Figure 10 indicates that the amorphous thickness (L_a), measured as the difference between the long period and longitudinal crystal size, decreases with f_a and shrinkage as one would intuitively expect. Linear crystallinity (X_L), as defined by the ratio of longitudinal crystal size to the long period, was also calculated from the x-ray data. Values range from 60–75% and increase with increasing yarn dimensional stability. Since these values are roughly double the conventionally measured crystallinities, it seems plausible that a great deal of lateral intercrystalline

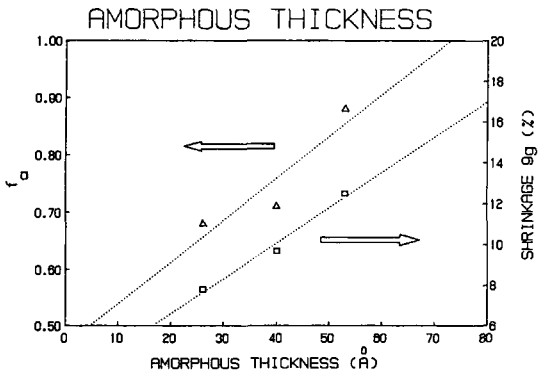

Figure 10 Plot of f_a and shrinkage under $9g$ load vs. amorphous thickness.

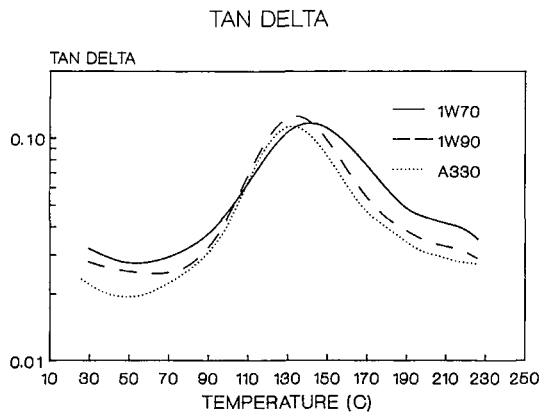

Figure 12 Plot of tan delta vs. temperature.

or interfibrillar amorphous regions exist. These regions can be envisioned to significantly contribute to intercrystalline connectivity thru tie chains. Others have also speculated about the importance of such a phase.[6,20]

The dynamic mechanical results are plotted in Figures 11 and 12. The storage modulus (E') exhibits the expected decrease centered at $\sim$ 130°C which corresponds to the glass transition temperature (T_g). It is interesting that the HMLS yarns possess the lowest room temperature modulus, consistent with previous results, yet retain a greater percentage of modulus above T_g. Since crystal structure tends to control properties above T_g, we suspect it is the greater linear crystallinity for these materials which causes this effect. It is not observed below T_g because amorphous orientation is the primary factor dictating properties. The low f_a and hence greater amorphous mobility for the HMLS products is believed to be responsible for lowering the temperature of the loss tangent maxima (Fig. 12).

At this point, the tenacity, modulus, and shrinkage characteristics have been explainable in terms of classical morphological analysis. However, an important question still remains. Why does A330, and to a lesser extent 1W90, possess high retractive force and significant stress-amplification? Clearly, some morphological characteristic, the exact nature of which is unknown at present, is giving rise to an elevated effective crosslink density. Perhaps the interfibrillar regions discussed above play a role. Research is continuing to clarify the origin this interesting phenomenon.

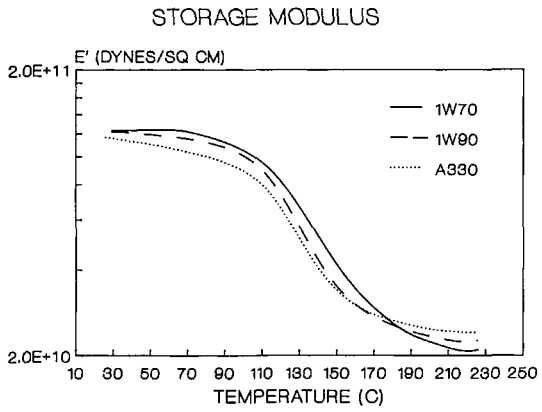

Figure 11 Plot of dynamic modulus vs. temperature.

SUMMARY

Classical morphological characteristics of yarns possessing a high degree of stress-amplification and low shrinkage have been identified. Tenacity, shrinkage, and initial modulus are primarily controlled by amorphous orientation, with increased orientation raising these parameters. The thickness of the amorphous regions also directly follows amorphous orientation. The degree of stress-amplification can be related to an "effective" crosslink density parameter as determined by application of rubber elasticity theory to retractive force vs. shrinkage plots. However, the exact morphological feature yielding this behavior is unknown. It is speculated that suppression of a yielding mechanism may be responsible for the observed stress-amplification. Study of the interfibrillar regions is a reasonable starting point for future investigation.

REFERENCES

1. R. J. Samuels, *Structured Polymer Properties,* Wiley-Interscience, New York, 1973, Ch. 4.

2. V. B. Gupta and S. Kumar, *J. Appl. Polym. Sci.*, **26,** 1877 (1981).
3. C. P. Buckley and D. R. Salem, *Polymer,* **28,** 69 (1987).
4. T. Kunugi, A. Suzuki, and M. Hashimoto, *J. Appl. Polym. Sci.*, **26,** 213 (1981).
5. P. N. Peszkin and J. M. Schultz, *J. Polym. Sci. Polym. Phys. Ed.*, **24,** 2591 (1986).
6. D. C. Prevorsek, G. A. Tirpak, P. J. Harget, and A. C. Reimschuessel, *J. Macromol. Sci. Physics,* **B9**(4), 733 (1974).
7. M. G. Northholt, A. Roos, and J. H. Kampschreur, *J. Polym. Sci. Polym. Phys. Ed.*, **27,** 1107 (1989).
8. T. Thistlethwaite, R. Jakeways, and I. M. Ward, *Polymer,* **29,** 61 (1980).
9. J. O. Warwicker and S. G. Graham, *J. Appl. Polym. Sci.*, **26,** 3045 (1981).
10. S. Fakirov, E. W. Fischer, R. Hoffmann, and G. F. Schmidt, *Polymer,* **18,** 1121 (1977).
11. S. Garg, *J. Appl. Polym. Sci.*, **27,** 2857 (1982).
12. F. Rietsch, *Eur. Polym. J.*, **21**(9), 793 (1985).
13. G. M. Bhatt and J. P. Bell, *J. Polym. Sci. Polym. Phys. Ed.*, **14,** 575 (1976).
14. B. Wunderlich, *Macromolecular Physics Vol. 3,* Academic, 1980. Ch. 8.4.5.
15. R. J. Young, *Introduction to Polymers,* Chapman and Hall, New York, 1983. Chap. 4.
16. R. de P. Daubeny, C. W. Bunn, and C. J. Brown, *Proc. R. Soc. London Ser.*, **A226,** 531 (1954).
17. H. G. Kilian, H. Halboth, and E. Jenckel, *Kolloid Z.*, **172,** 166 (1960).
18. R. J. Samuels, *J. Appl. Polym. Sci.*, **10,** 781 (1972).
19. J. H. Dumbleton, *Polymer,* **10,** 539 (1969).
20. G. Lemanska and A. Narebska, *J. Polym. Sci.*, **18,** 917 (1980).
21. P. B. Rim, *J. Macromol. Sci. Phys. Ed.*, **B26**(1), 19 (1987).
22. J-I Wang and I. R. Harrison, *Methods of Experimental Physics,* R. A. Fava, Ed., Academic, 1980, Ch. 6.

Received February 18, 1990
Accepted June 20, 1990